J. theor. Biol. (1997) **184,** 441–450

A Hydrodynamic model for *Dictyostelium discoideum* Mound Formation

BAKHTIER VASIEV,* FLORIAN SIEGERT and CORNELIS J. WEIJER*†

Zoologisches Institut, Universität München, Luisenstraße 14, 80333 *München, Germany*

(*Received on* 30 *May* 1996, *Accepted in revised form on* 27 *September* 1996)

Coordinated cell movement is the major mechanism controlling the multicellular morphogenesis of the slime mould *Dictyostelium discoideum*. Single cells aggregate chemotactically in response to propagating waves of cAMP to form a multicellular organism. Here we present a model to describe the formation of these multicellular aggregates. Cell movement is modelled as the flow of a compressible fluid controlled by cAMP-induced chemotactic forces, frictional and adhesion forces and internal pressure. The model can simulate the whole early process of development from isolated single cells, formation of bifurcating aggregation streams and formation of a three-dimensional aggregate with a single set of parameters. Direct comparison of simulations with experimental images of successive aggregation stages show a striking agreement. The model can also mimic alternative modes of morphogenesis frequently observed after disturbance of cAMP signalling or cell motility by chemicals or mutations.

Introduction

Dictyostelium morphogenesis is initiated by chemotactic aggregation of free living single amoebae into multicellular aggregates (mounds) (Loomis, 1982; Firtel, 1995; Chen *et al*., 1996). During further development the initially homogenous cell population differentiates into several cell types and forms a fruiting body consisting of stalk and spore cells. Aggregation is mediated over large distances by travelling waves of the chemo-attractant 3′–5′cyclic-Adenosine-mono-phosphate (cAMP) emitted periodically by the aggregation centre. The cells respond to these cAMP waves with periodic chemotactic motion towards the signal source. In the course of aggregation the cells encounter a diverse range conditions. Initially the cells are widely dispersed over the substrate and cell density is low. After 10–15 waves the cells begin to concentrate and form aggregation streams in which they form cell–cell contacts. Due to the progressive accumulation of cells, the aggregate extends upwards from the substrate and forms a three-dimensional hemispherical structure, the mound.

There have been a number of models describing early *Dictyostelium* development, i.e. the two-dimensional aggregation of randomly distributed cells in aggregation streams. In one class of models the amoebae are described as cellular automata (Vasieva *et al*., 1994), in hybrid models the cells are described as automata, but the chemical reaction kinetics are treated as continuous (Kessley & Levine, 1993), while in still other models the cells are treated as a continuous density function (Vasiev *et al*., 1994; Höfer *et al*., 1995). These models have been studied numerically and analytically and the principal mechanisms responsible for stream formation are now clear (Levine & Reynolds, 1991; Vasiev *et al*., 1994).

There is good experimental evidence that the same principles that control aggregation, cAMP wave propagation, and chemotactic cell movement also control the formation and morphogenesis of the mound (Siegert & Weijer, 1995). However, mound formation has not yet been modelled in any detail as cells reach high densities in the mound and a good description of cell movement should take cell–cell

*Present address: Department of Anatomy & Physiology, Old Medical School, University of Dundee, Dundee, DD1 4HN, U.K.
†Author to whom correspondence should be addressed.

0022–5193/97/040441 + 10 $25.00/0/jt960282

interactions into account. The models mentioned above do not consider these interactions and, as a result the final structures obtained are either a flat collection of cells or regions occur where cell density tends to infinity. An early ingenious approach to model cell movement at high cell density was suggested by Odell & Bonner (1986), who attempted to model cell movement during slug migration as a fluid flow using Navier–Stokes equations. We show here that a similar approach can be used to describe early development until mound formation. Our model is based on chemotactic signal propagation in an excitable medium (Tyson *et al.*, 1989; Tang & Othmer, 1995; Siegert & Weijer, 1995) and chemotactic cell movement is modelled as the flow of a compressible fluid. The system is self-organizing, going from randomly distributed single cells via bifurcating aggregation streams to the formation of a three-dimensional mound.

Model

To model the excitable cAMP kinetics we use the FitzHugh–Nagumo equations:

$$\partial g/\partial t = D\Delta g - \alpha\rho(k_g g(g-0.05)(g-1) + k_r r) \quad (1)$$

$$\partial r/\partial t = (g-r)/\tau \quad (2)$$

where g defines the level of extracellular cAMP, and r the state of the cAMP receptors. D is the diffusion coefficient for cAMP; τ is a time scaling factor for the variables r and g; k_g and k_r define the rate of production and hydrolysis of cAMP by one cell. Locally, the cAMP kinetics is proportional to the density of cells ρ (Kessler & Levine, 1993; Vasiev *et al.* 1994). Factor α defines the fraction of cells involved in the production and decay of cAMP.

Cell movement is described by the Navier–Stokes equation (Landau & Lifshitz, 1963):

$$\rho[\partial \mathrm{V}/\partial t + (\mathrm{V}\nabla)\mathrm{V}] = \mathrm{F_{ch}} + \mathrm{F_{fr}} + \eta\Delta\mathrm{V} + (\xi + \eta/3)\mathrm{grad}\,div\,\mathrm{V} + \mathrm{F}_{ad} - \mathrm{grad}\rho \quad (3)$$

The left-hand side of the equation describes the acceleration of the cells under the influence of various forces described in the right-hand side of the equation. V is the velocity of the cells. F_{ch} is the chemotactic force which is active on the front of cAMP waves, F_{fr} is a friction force responsible for slowing down cell movement. The third and fourth terms on the right-hand side describe cell–cell friction: η and ξ are viscosity coefficients. F_{ad} takes into account cell–cell and cell–substrate adhesion forces, ρ is the pressure between the cells caused by the chemotactic accumulation of the cells (see appendix B for details).

The change in cell density over time is calculated from the equation of conservation of mass (Landau & Lifshitz, 1963; Murray, 1989):

$$\partial\rho/\partial t = \mathrm{D}\rho\Delta\rho - div(\rho\mathrm{V}) \quad (4)$$

The first term on the right-hand side of the equation describes the random motion of the cells, while the second term describes co-ordinated movement.

Calculations were performed in a three-dimensional $100 \times 100 \times 20$ array using the explicit method, that is, forward time-centred space method for the diffusion term and the upwind method for the advective term (details in Appendix A). Both methods are stable with given space and time steps ($h_x = 0.4$; $h_t = 0.01$), diffusion coefficients ($D = 0.1$; $D_\rho = 0.0005$) and maximal value of chemotactic flow ($max|\mathrm{V}| < 5.$ in all the computations). For the cAMP concentration field we used von Neumann's "no flux" boundary conditions at the boundary of the medium as well as at the free boundary of the mound. The same conditions have also been imposed on the cell density field. The value of the cells velocity was set to zero at the medium boundary as well as in the space outside of the free boundary of the mound (see Appendix B for details about the definition of the mounds free boundary).

To describe the excitable medium we have used the following basic set of parameters $\tau = 5.$; $k_g = 10.5$; $k_r = 3$; $\alpha = 1.$; $D = 0.1$. The refractoriness of the medium where the density of cells is still uniform ($\rho = 0.5$) is equal to 20 time units and the velocity of the cAMP waves is 0.3 space units per time unit. Since in natural populations of aggregating *Dictyostelium* cells the refractoriness is about 5 min and the velocity of cAMP waves is 600 μm/min (Siegert & Weijer, 1989) our time unit is 15 s and the space unit is 500 μm. Values of the chemotactic and frictional forces (given in Appendix B) have been chosen such that the cells' average velocity at the stage of stream formation was 2–4% of the cAMP wave velocity. The "diffusion" coefficient in (4) has been chosen such that the formation of aggregation streams takes place after propagation of 15–20 cAMP waves, similar to experimental observations (Siegert & Weijer, 1989). For example, an increase in the rate of the cells' random motion ($D_\rho = 0.001$) leads to an increase in stream formation time (about 25 cAMP waves). Values of the pressure and adhesive forces have been chosen such that we obtain roughly hemispherical mounds (see Appendix C).

We have used two versions of the model corresponding to non-viscous and viscous cell flows.

We assumed that initial stage of aggregation where the cells are still mostly single, i.e. where there are few cell–cell interactions, can be best described by a non-viscous flow model, while later, at the mound stage where cell–cell interactions are prominent, can best be described by a viscous flow model. For a more further description of the properties of these two models see Appendices B and C.

Results

MOUND FORMATION

Using the model for non-viscous cell flows we simulated morphogenesis up to the mound stage. We initiate a spiral cAMP wave in the centre of a two-dimensional field of randomly distributed cells [Fig. 1(A)]. This wave causes periodic changes in cell movement and results in the formation of aggregation streams [Fig. 1(B)]. Bifurcating aggregation streams form due to the dependence of wave propagation speed on the cell density (Levine & Reynolds, 1991; Vasiev *et al*., 1994). As more cells move towards the centre, a hemispherical mound forms [Fig. 1(C,D)]. The pressure p developing between the cells as a result of chemotactic accumulation of the cells is responsible for mound formation. It increases during aggregation and forces the cells up into the third dimension. The aggregation patterns observed in the simulations are remarkably similar to those from real experiments [compare Fig. 1(A–D) with Fig. 1(E–H)]. Experiments have shown that during aggregation there is a decrease in the period and propagation speed of cAMP waves, which results in a decrease in the wavelength of the spiral wave (Gross *et al*., 1976; Siegert & Weijer, 1989). This behaviour is also observed in the model calculations [Fig. 1 (A–D)].

FORMATION OF A CELL FREE CORE DURING EARLY AGGREGATION

In experiments we often observed the formation of a cell-free region around which the tip of the cAMP spiral rotated (Siegert & Weijer 1989). This region delineates the core of the cAMP spiral wave. During development this cell-free region gradually collapses, a behaviour seen also in the simulations [Fig. 1(A–D)]. The occurrence and collapse of the cell-free region can be explained by the dependence of the size of the spiral core on the excitability of the medium. Initially, during early aggregation, cell density is low, therefore the medium has a low excitability and the core of the spiral is large. Cells in the core of the spiral wave move outward towards the tip of the spiral resulting in the formation of a cell-free region. During later aggregation more cells enter the aggregation streams and accumulate on a loop around the core. This increase in local cell density leads to an increase in the excitability, leading to a decrease of the diameter of the spiral core until the cell-free region disappears completely.

Decreasing the excitability in the computer simulations by varying the rate of cAMP production leads to a large cell-free region in the centre of the aggregates [Fig. 2(A,B)]. Decreasing excitability experimentally by inhibiting cAMP production with caffeine (Brenner & Thoms, 1984; Siegert & Weijer, 1989) also leads to a large cell-free region in the centre of the aggregate [Fig. 2(C,D)]. Unexpectedly the simulations also showed that large cell-free cores appear if the movement velocity of the cells is increased [Fig. 2(E,F)]. We suspect that an increase in movement velocity leads to a decrease in the local cell density in the front of the wave thereby decreasing the excitability of the medium. Although there is not yet any experimental evidence for this mechanism of formation of cell-free cores it is worth investigating this possibility experimentally in mutants with impaired cell movement.

MEANDERING MOUNDS

The simulations show that in mound the spiral tip (scroll filament) is located in the centre and the mound is stationary [Fig. 3(A)]. However, if the excitability of the medium is decreased, the spiral becomes non-stationary and drifts away from the centre of the mound [Fig. 3(B)]. The spiral tip describes a meandering motion. As a consequence the mound begins to move over the surface on a circular trajectory. This circular motion is seen as meandering of the mound position in a time–space plot [Fig. 3(C)]. Stationary mounds are normally observed in the wild type strains [Fig. 3(D)] and the tip of the spiral wave, visualized as an optical density wave, is stably located in the centre of such mounds leading to rotational cell movement (Siegert *et al*., 1994; Siegert & Weijer, 1995). We have also observed non-stationary mounds in a streamer mutant (Streamer F), which is defective in cGMP phosphodiesterase (Ross & Newell, 1981). We therefore investigated the propagation of darkfield waves in these mutants and found that the tip of the spiral is located laterally in the mound [Fig. 3(E)] as in the simulations. The circular movement of the mound, as in the simulations, is seen as a meandering of the mounds position in the time–space plot [Fig. 3(F)].

TRANSFORMATION OF MOUNDS TO RINGS

If in simulations the kinetics of the cAMP signal is gradually decreased further the meandering stops and the mounds transforms into a ring-shaped structure with increasing diameter [compare Fig. 3(B) with Fig. 4(A–C)]. The cAMP spiral core increases and the cells inside the spiral core follow the tip and move from the centre as during aggregation. As a result the mound gradually transforms to a ring with nearly no cells in the centre. The cAMP waves continue to rotate around the ring giving rise to counter-rotational cell movement. We found that mounds of the streamer F mutant can also open up and transform into a ring [Fig. 4(D–F)] similar to the simulations. Although there is as yet no experimental evidence that streamer F mounds have a reduced excitability *in vivo* the model calculations suggest this to be the case and this should be investigated experimentally.

To model changes in the population excitability we varied parameter k_g (Fig. 2). Decrease of this parameter simulates the decrease in amount of cAMP released by cells, as is the case with caffeine. In the simulations presented in Figs 3 and 4 we have decreased the excitability of the medium by decrease of the model parameter α, which describes the fraction of cells releasing cAMP. This could reflect differentiation of cells into relaying and non-relaying cell types (Bretschneider *et al*., 1995). However the main effect of the variations of these two parameters (k_g and α) is a change in the medium's excitability, therefore both parameters can be used to reproduce all the phenomena reported here.

Discussion

CONSIDERING CHEMOTACTIC CELL MOVEMENT AS A FLUID FLOW

Slime mould morphogenesis results from propagation of cAMP waves which control the chemotactic movement of individual amoebae. To describe the behaviour of this population of cells some simplifying assumptions have to be made. The main assumption made in this paper is that cell movement can be considered as the flow of a liquid. In this approach the cell–cell interactions are taken into account by pressure, adhesion and viscosity terms. There are several arguments for why it is reasonable to view a population of cells as a continuous liquid. During early aggregation when the cells are still single, they exhibit directed motion during the rising phase of the wave and random motion during the rest of the time. As soon as the cells enter aggregation streams their rate of movement becomes almost constant in time, despite the periodic nature of the chemotactic signal (Siegert & Weijer, 1995; Rietdorf *et al*., 1996). The cells do not slow down significantly between chemotactic waves. This implies that there are strong interactions between the cells, although they do not have fixed neighbours. The cells make and break contacts continuously. Furthermore, cells in mounds,

FIG. 1. Development of *Dictyostelium* from single cells to the mound stage. (A–D) successive images of aggregation as calculated by the model (E–H) Photographs taken at successive times during development of strain Ax-2 (at 0, 3, 6, 9 h of development). Bar in E = 5 mm and in (F,G,H) = 500 μm. In the simulations cell density is shown as a yellow iso-surface ($\rho = 0.5$) and the cAMP concentrations are mapped on this surface from low cAMP (blue, $g = 0$) to high cAMP (red, $g = 0.8$). The initial density of cells was zero everywhere in 3d-space except for the bottom plane. The cell density in each grid of this plane was represented by a random number varying between 0 and 1 so that average density in this plane was equal to 0.5. The mound in (D) is close to its final stable shape.

FIG. 2. Effects of changes in excitability and rate of cell movement on morphogenesis. (A,B) Core formation depend on the rate of the cAMP production in simulations. All the model parameters except the ones noted below are the same as in Fig. 1. The rate of cAMP production has been changed by variation of k_g. In (A) the rate of cAMP production is increased ($k_g = 11$) and in (B) decreased ($k_g = 10$). (C,D) Aggregation of Ax-2 in the absence (C) or presence (D) of 3 mM caffeine. Caffeine results in an increase of the size of the core in the centre of the aggregate at 6 h of development. Bar: 200 μm. (E,F) Change in core size observed in simulations as a result of a change in cell velocity. The velocity has been changed by variation of chemotactic force. $K_{ch} = 0.1$ in (E) and $K_{ch} = 0.3$ in (F).

FIG. 3. Meandering mounds in simulations and experiment. Top view of a stationary mound in the simulation (A) and in the strain Ax2 (D), both showing a spiral wave (projection of a scroll wave) with the core located at the centre of the mound. As an initial condition in (A) we used a hemispherical mound (the density of the cells is equal 1 inside of the mound and 0 outside) where a scroll wave was initiated. The shape of the mound in (A) is stable. Bar in (D) is 200 μm. (B,E) Meandering mound in the simulations (b) and in the streamer F mutant NP368 (E), both showing a spiral wave whose centre does not coincide with the centre of the mound. (C,F) Time–space plot showing a section of a meandering mound over time in the simulations (C) and in strain NP368 (F). The time–space plots were constructed reading out the optical density along a horizontal line through the image of the mound (E). This process was repeated for successive time points and the resulting sections lined up one below the other in a "time–space" plot. In the computations the time–space plot (C) was constructed by reading out ($\rho + 0.2|V|$) along a line on the bottom plane of the mound (B). Propagating waves are now visible as blue/red (C) or dark tilted (F) bands. The section is 60 grids in (C) and 400 μm in (F). To construct the time–space plot in (C) 120 sections were taken every 5 time units, and 512 images taken at 10 s for the plot in (F). In the graphs the path of the meandering mound translates into an oscillatory path. $\alpha = 1$ in (A) (all cells relay cAMP); and $\alpha = 0.75$ in (B,C) (75% of the cells relay cAMP).

FIG. 4. Transformation of a mound into a ring. (A–C) A sequence showing ring formation from a mound obtained by lowering the excitability and cell movement speed. The same model and parameters as in Fig. 3 were used, except for α which is changed gradually from 0.6 in (A) to 0.475 in (C). (D–F) Transformation of a mound to a ring as observed in the streamer F mutant NP377. Time in (D) 0 min, (E) 30 min, (F) 40 min. Bar = 450 μm.

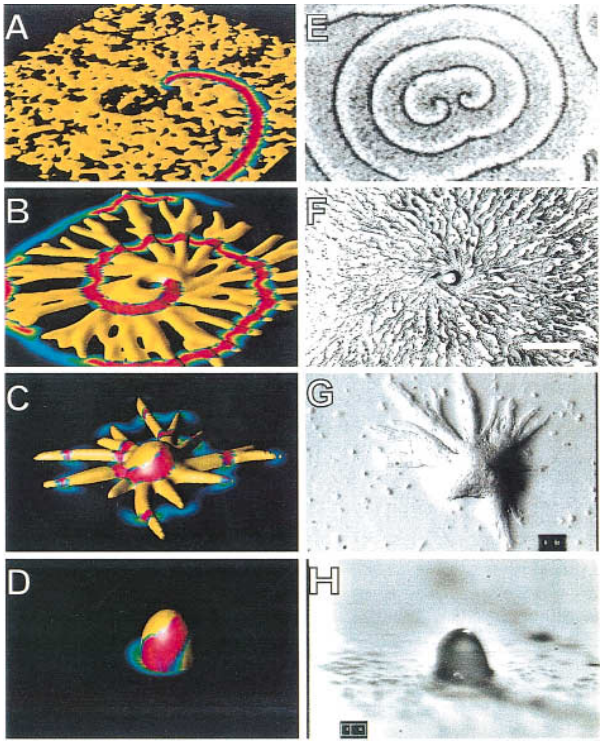

FIG. 1.

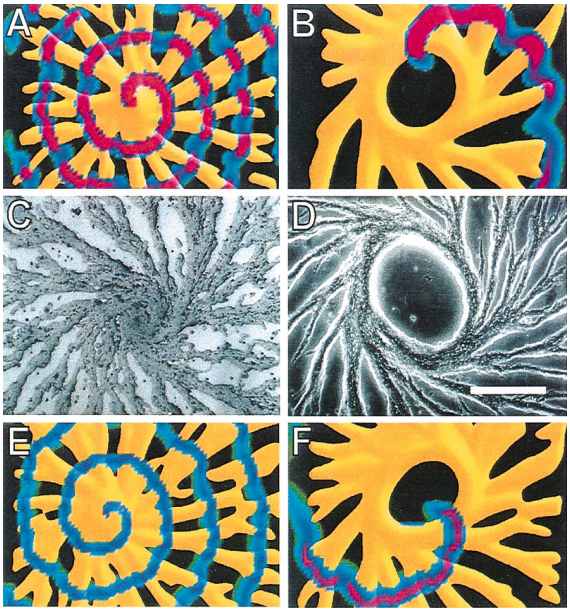

FIG. 2.

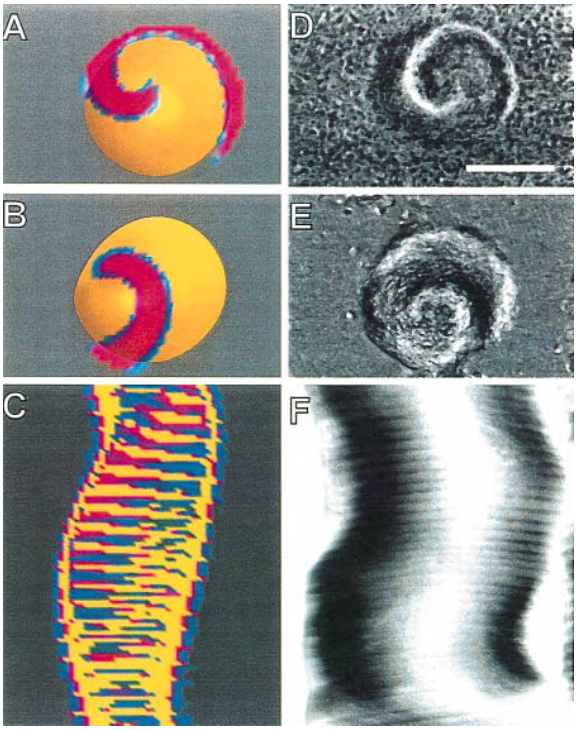

FIG. 3.

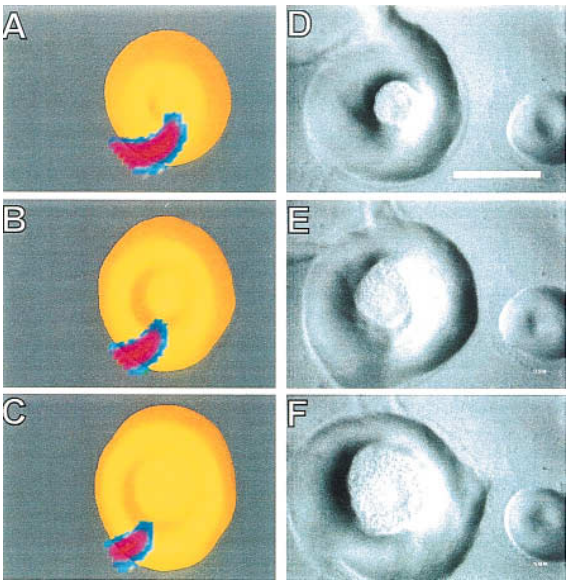

FIG. 4.

which rotate around a central core, show a velocity profile that is smooth in space. The velocity is maximal in the middle between the centre of the mound and the periphery (Siegert *et al*., 1994; Siegert & Weijer, 1995). These properties are similar to those of a viscous liquid.

SIMPLIFYING ASSUMPTIONS MADE IN THE MODEL

We realize that the model simplifies the processes of mound formation in several aspects. 1. In real life the amoebae are separate entities whose individual properties are fluid-like and which are moving in an extracellular matrix that also might be considered as a viscous liquid. As a simplification we consider this complex system as a uniform liquid. 2. In our model cell–cell and cell–substrate adhesion is simply taken into account as a force that holds the cell density inside the mound nearly constant and is directed downwards to the substrate. This is a reasonable assumption as a first approximation, but the description can be improved by more detailed considerations of surface tension and liquid–substrate adhesion. 3. The mound is covered by a slime sheath, a physical barrier that is continually synthesized and is clearly deformable, but whose exact mechanical properties are not clear. The slime sheath is stationary with respect to the substratum and will influence the motion of nearby amoebae. We have considered the effect of the slime sheath as that of a stationary barrier covering the mound boundary. Detailed properties of slime sheath and its influence on the motion of the amoebae should be studied experimentally before they can be considered in a model in any detail. 4. We consider mound formation as compacting of a compressible liquid. However, the mound itself is incompressible and in order to describe slug formation the system should be considered as an incompressible liquid. This assumes that density is constant and involves computations of the mound shape changes.

MEANDERING OF MOUNDS

Spiral waves meander in high excitable media, when the period of their rotation is smaller than the refractoriness of the medium (Muller & Zykov, 1994). In our computations presented in Fig. 3 the spiral starts to meander when the excitability of the medium decreases. The mechanism of meandering in this case is the following. A decrease in excitability leads to an increase in the size of the spiral core. Since the spiral tip rotates around a larger core it comes closer to the mounds boundary and this destabilizes its motion. The boundary of the mound attracts the spiral. This was shown in two types of computations (1) in a 2d-medium, inhomogeneous in cell density, spirals drift in the direction of lower cell density; (2) in a mound consisting of low excitable non-motile cells, a spiral drifts in the direction of the mound boundary and disappears. However, due to the chemotactic motion of the cells which try to follow the spirals tip, the mound shifts. This results in a change of direction of the spiral drift, leading to meandering of the spiral and the mound.

BIOLOGICAL IMPLICATIONS OF THE MODEL

The calculations clearly show that it is possible to describe the process of mound formation by usage of a constant set of parameters without additional assumptions concerning evolution of the system parameters (Fig. 1). The mound is the final stable solution in this system. This implies that this complicated process could take place without the necessity for transcription of new genes. In real life, however, it is known that many different genes are transcribed during aggregation and mound formation. Essential components of the cAMP signal relay system such as cAMP receptors, G proteins, phosphodiesterase and adenylyl cyclase all increase considerably during development (Firtel, 1995). The expression of these genes is under feedback control of the cAMP pulses (Gerisch, 1987). This may provide extra stability to the system as well as fine tuning of the process. However, to proceed in morphogenesis to the slug stage new qualities need to be added to the model, like different cell types with different cAMP relay kinetics and movement properties.

The model also provides insight into some more complex behavioural modes of mounds, like meandering and ring formation. The calculations show that these properties depend on the cAMP kinetics. These predictions can now be tested experimentally by investigation of mutants in known components of the signal transduction system that should show altered kinetics. Mutants to investigate are receptor mutants with a reduced affinity for cAMP which makes the system less sensitive (Johnson *et al*., 1993; Caterina *et al*., 1994), as well as mutants in the cAMP hydrolysing enzyme cAMP phosphodiesterase (Hall *et al*., 1993). Mutants with reduced phosphodiesterase should show reduced rates of cAMP degradation and therefore a decreased rate of resensitization. This work shows that it is possible to understand aggregation and mound formation of *Dictyostelium* on the basis of well-known physico-chemical principles. Furthermore, these model calculations help in understanding apparently complex biological phenotypes and direct new experiments.

We gratefully acknowledge the Alexander von Humboldt Foundation for a research fellowship to Bakhtier Vasiev. We thank Dr Charles N. David for comments on the manuscript. This work was supported in part by grants of the Deutsche Forschungsgemeinschaft (We1127).

REFERENCES

Barkley, D., Kness, M. & Tuckerman, L. S. (1990). Spiral wave dynamics in a simple model of excitable media. *Phys. Rev. A.* **42,** 2489–2492.

Brenner, M. & Thoms, S. (1984). Caffeine blocks activation of cyclic AMP synthesis in *Dictyostelium discoideum*. *Dev. Biol.* **101,** 136–146.

Bretschneider, T., Siegert, F. & Weijer, C. J. (1994). Three dimensional spiral cAMP waves direct cell movement and gene expression in *Dictyostelium* slugs. *Proc. Natl Acad. Sci. USA* **92,** 4387–4391.

Caterina, M. J., Milne, L. L. S. & Devreotes, P. N. (1994). Mutation of the third intracellular loop of the cAMP receptor, cAR1, of *Dictyostelium* yields mutants impaired in multiple signaling pathways. *J. Biol. Chem.* **269,** 1523–1532.

Chen, M. Y., Install, R. H. & Devreotes, P. N. (1996). Signaling through chemoattractant receptors in *Dictyostelium*. *TIG* **12,** 52–57.

Firtel, R. A. (1995). Integration of signaling information in controlling cell-fate decisions in *Dictyostelium*. *Gene Dev.* **9,** 1427–1444.

Gerisch, G. (1987). Cyclic AMP and other signals controlling cell development and differentiation in *Dictyostelium*. *Ann. Rev. Biochem.* **56,** 853–879.

Gross, J. D., Peacey, M. J. & Trevan, D. J. (1976). Signal emission and relay propagation during early aggregation in *Dictyostelium discoideum*. *J. Cell Sci.* **22,** 645–656.

Hall, A. L., Franke, J., Faure, M. & Kessin, R. H. (1993). The role of the cyclic nucleotide phosphodiesterase of *Dictyostelium discoideum* during growth, aggregation, and morphogenesis: overexpression and localization studies with the separate promoters of the pde. *Dev. Biol.* **157,** 73–84.

Höfer, T., Sherrat, J. A. & Maini, P. K. (1995). *Dictyostelium discoideum*: cellular self-organization in an excitable biological medium. *Proc. R. Soc. Lond. B* **259,** 249–257.

Johnson, R. L., Van Haastert, P. J. M., Kimmel, A. R., Saxe III, C. L., Jastorff, B. & Devreotes, P. N. (1992). The cyclic nucleotide specificity of three cAMP receptors in *Dictyostelium*. *J. Biol. Chem.* **267,** 4600–4607.

Kessler, D. A. & Levine, H. (1993). Pattern formation in *Dictyostelium* via the dynamics of cooperative biological entities. *Phys. Rev. E.* **48,** 4801–4804.

Landau, L. & Lifshitz, E. (1963). *Fluid Mechanics*. New York: Pergamon Press.

Levine, H. & Reynolds, W. (1991). Streaming instability of aggregating slime mold amoebae. *Phys. Rev. Lett.* **66,** 2400–2403.

Loomis, W. F.(1982). *The Development of* Dictyostelium discoideum. New York: Academic Press.

Murray, J. D. (1989). *Mathematical Biology*. Berlin: Springer-Verlag.

Muller, S. C. & Zykov, V. S. (1994). Simple and complex spiral wave dynamics. *Phil. Trans. R. Soc. Lond. A* **347,** 677–685.

Odell, G. M. & Bonner, J. T. (1986). How the *Dictyostelium discoideum* grex crawls. *Phil. Trans. R. Soc. Lond. B* **312,** 487–525.

Press, W. H., Flannery, B. P., Teukolsky, S. A. & Vetterling, W. T. (1988) *Numerical Recipes in C*. Cambridge: Cambridge University Press.

Rietdorf, L., Siegert, F. & Weijer, C. J. (1996). Analysis of optical density wave propagation and cell movement during mound formation in *Dictyostelium discoideum*. *Dev. Biol.* **177,** 427–438.

Ross, F. M. & Newell, P. C. (1981). Streamers: chemotactic mutants of *Dictyostelium discoideum* with altered cyclic GMP metabolism. *J. Gen. Microbiol.* **127,** 339–350.

Siegert, F. & Weijer, C. J. (1989). Digital image processing of optical density wave propagation in *Dictyostelium discoideum* and analysis of the effect of caffeine and ammonia. *J. Cell Sci.* **93,** 325–335.

Siegert, F., Weijer, C. J., Nomura, A. & Miike, H. (1994). A gradient method for the quantitative analysis of cell movement and tissue flow and its application to the analysis of multicellular *Dictyostelium* development. *J. Cell. Sci.* **107,** 97–104.

Siegert, F. & Weijer, C. J. (1995). Spiral and concentric waves organize multicellular *Dictyostelium* mounds. *Curr. Biol.* **5,** 937–943.

Tang, Y. H. & Othmer, H. G. (1995). Excitation, oscillations and wave propagation in a G-protein-based model of signal transduction in *Dictyostelium discoideum*. *Phil. Trans. R. Soc. Lond. B.* **349,** 179–195.

Tyson, J. J., Alexander, K. A., Manorajan, V. S. & Murray, J. D. (1989). Spiral waves of cyclic AMP in a model of slime mold aggregation. *Physica* **34D,** 193–207.

Vasiev, B. N., Hogeweg, P. & Panfilov, A. V. (1994). Simulation of *Dicttyostelium discoideum* aggregation via reaction-diffusion model. *Phys. Rev. Lett.* **73,** 3173–3176.

Vasieva, O. O., Vasiev, B. N., Karpov, V. & Zaikin, A. N. (1994). A model of *Dictyostelium* aggregation. *J. theor. Biol.* **171,** 3561–367.

APPENDIX A

Numerical Schemes

For integration of all eqns (1–4) we have used explicit numerical methods. The diffusion terms in (1), (3), and (4) were discretised by the FTCS (forward time centred space) method using 18 neighbouring points in 4d-space. That is, the Laplacian operator was calculated as following:

$$\Delta u = (4(u_{i+1,j,k} + u_{i-1,j,k} + u_{i,j+1,k} + u_{i,j-1,k} + u_{i,j,k+1} + u_{i,j,k-1})0 + u_{i+1,j+1,k} + u_{i-1,j+1,k} + u_{i+1,j-1,k} + u_{i-1,j-1,k} + u_{i+1,j,k+1} + u_{i+1,j,k-1} + u_{i-1,j,k+1} + u_{i-1,j,k-1} + u_{i,j+1,k+1} + u_{i,j+1,k-1} u_{i,j-1,k+1} + u_{i,j-1,k-1} - 36u_{i,j,k})/(8h_x^2)$$

where u can represent the cAMP level in (1), any component of flow velocity in (3), or cell density in (4). This scheme is a three-dimensional (3d) version of the scheme suggested by Barkley (1990) for the calculation of the 2d Laplacian. This scheme is much more isotropic than the classical one which uses six neighbours ($u_{i\pm1,j,k}$, $u_{i,j\pm1,k}$, and $u_{i,j,k\pm1}$). Since in the system under consideration, there is a principal instability (''streaming instability'', Levine & Reynolds, 1991) we have to use numerical schemes which keep wave velocity constant in all the directions and thereby prevent the formation of artificial streams. Used scheme is stable when: $D_u h_t/h_x^2 < 1/6$

where D_u means either diffusion coefficient of cAMP in (1), or viscosity coefficient in (3), or coefficient of cell random motion in (4). In all these cases this condition has been satisfied in our computations.

The term grad*div*V in (3) leads to the occurrence of a number of second velocity derivatives ($\partial/\partial x_k(\partial v_l/\partial x_l)$). They were all discretised by the FTCS method:

$$\partial^2 u/\partial x^2 = (u_{i+1,j,k} + u_{i-1,j,k} - 2u_{i,j,k})/h_x^2$$

$$\partial^2 u/\partial x\partial y = (u_{i+1,j+1,k} + u_{i-1,j-1,k} - u_{i+1,j-1,k} - u_{i-1,j+1,k})/(4h_x^2)$$

The condition for stability of these schemes $D_u h_t/h_x^2 < 1/2$ has also been satisfied.

First-order velocity and cAMP derivatives have been calculated as following:

$$\partial u/\partial x = (u_{i+1,j,k} - u_{i-1,j,k})/(2h_x)$$

which was also stable for the values of time and space steps used and in the range of density and velocity changes that occurred during the computations ($A^*h_t/h_x < 1$ where A is either velocity or density of cells). To avoid anisotropy in the obtained patterns which arise during computations due to the anisotropy in the discretization schemes we alternated the set of neighbours used in these schemes for each second iteration step. The schemes given above were used for odd iteration steps. For even iteration steps we used the following:

$$\partial u/\partial x = (u_{i+1,j+1,k} + u_{i+1,j-1,k} - u_{i-1,j+1,k} - u_{i-1,j-1,k})/(4h_x)$$

$$\partial^2 u/\partial x^2 = (u_{i+1,j+1,k} + u_{i-1,j-1,k} + u_{i+1,j-1,k} + u_{i-1,j+1,k} - 4u_{i,j,k})/(2h_x^2)$$

This alternation of schemes was very efficient to avoid anisotropy effects in the patterns obtained. We did not alternate the scheme for $\partial^2 u/\partial x\partial y$ as we did not find a good alternative scheme. The problem of anisotropy, however, was satisfactorily solved by alternation of two other schemes.

The first order derivatives of density in (4) were discretized using the explicit upwind method:

$$\partial\rho/\partial x = (\rho_{i+1,j,k} - \rho_{i,j,k})/h_x \text{ if } v_{i,j,k} > 0;$$

$$\partial\rho/\partial x = (\rho_{i,j,k} - \rho_{i-1,j,k})/h_x \text{ otherwise,}$$

where $v_{i,j,k}$ is the x-component of the cells velocity in the space grid considered. This scheme is the simplest one which can be used for stable integration of the equation of conservation of mass (Press *et al*., 1988). The condition for its stability, $A^*h_t/h_x < 1$, where A is a value of any velocity component at any time during the computation, has been satisfied. Using this scheme we were able to integrate equation (4) without substantial changes (not more than 10%) in the total number of cells (integral of the density of cells over the whole volume) during the computations.

Using the discretisation schemes given above we have found that the values of the model parameters (given in the "Model" section of the paper) give rise to stable computations using $h_x = 0.4$ and $h_t = 0.01$. Increasing the space or time steps led to a destabilization of the computations. The computation presented in Fig. 1 (2×10^5 iteration steps in a medium of $100 \times 100 \times 20$ grids) took about 25.5 h of CPU time on an IBM RS 6000 model 350 workstation. This computation has been made using the non-viscous flow version of the model which is almost three times faster than viscous flow model.

APPENDIX B

Details of the Model

DEFINITION OF THE MOUNDS-FREE BOUNDARY

One of the main challenges in these computations is to describe the behaviour of the mounds surface as it is a free moving boundary. The boundary was defined as a surface consisting of grid points where the cells' density changes from $\rho > \rho_{th}$ to $\rho < \rho_{th}$ where $\rho_{th} = 0.5$. The value 0.5 was taken arbitrary and can vary in a range from 0.8 to 0.3 without essential influence on the results. Near the mound boundary we have used some restrictions for cell movement:

1. There is no random motion of the cells in an empty grid, that is, cells cannot cross the boundary during random movement.
2. Cells can only flow into grids where $\rho > \rho_{th}$ or which have at least one neighbouring grid where $\rho > \rho_{th}$. This rule allows the mound to change its shape, for example, to elongate due to pressure.
3. On the medium boundary the velocity of the cells is zero. In the grids where $\rho < \rho_{th}$ and which are surrounded by grids which all satisfy this condition the velocity of the cells is also supposed to be zero. This results in a non-motile space surrounding the mound, i.e. there is a non-motile layer covering the mounds free boundary.

These assumptions lead to a steep change in cell density at the mound boundary (2–3 grid points to decrease the cell density from around 1 to 0). Thus,

although we use a continuum model to describe mound formation, due to these restrictions for cell movement we obtain a well-defined mound.

The no-flux boundary condition for cAMP field on the free boundary of mound has been implemented as follows. The cAMP level is calculated according to (1) in the grids where $\rho > \rho_{th}$. This value is copied to the upper grid if $\rho < \rho_{th}$. In all the other grids cAMP level has been set to zero. This algorithm results in a cAMP surface covering the mound leading to no flow of cAMP on the surface of the mound. Using this method we did not find a detectable influence of the mounds boundary on the cAMP waves inside the mound. This was the simplest scheme of a few others which also could be used. A similar method has been used to avoid random motion of cells through the mounds-free surface.

NON-VISCOUS FLOW MODEL

In the computations presented in Figs 1 and 2 we have used the Euler equation rather than the Navier–Stokes equation, i.e. we have neglected the effect of viscosity: $\eta = 0$ and $\xi = 0$. To calculate cell flow velocity we assumed:

(a) The chemotactic force occurs only at the front of the wave: $F_{ch} = \rho K_{ch} \mathrm{grad} g$ where $K_{ch} = 0$ when $\partial g/\partial t \leq 0$ and $K_{ch} = 0.2$ when $\partial g/\partial t > 0$. To distinguish the wave front and the wave back we used the sign of cAMP time derivative rather than state of cAMP receptors (Vasiev *et al*., 1994; Höfer *et al*., 1995). Using the state of the cAMP receptors to control cell movement always resulted in an instability of the spiral wave rotation, since the receptor relaxation time increases with increasing cell density. When a spiral rotates with a period close to the refractoriness of the medium the motion of cells in regions with a lower cells density is essentially longer than that of cells in regions of high density. This results in multiple breaks in aggregation streams and in the ring of cells formed by the spiral tip.

(b) Cell movement is slowed down by a "friction" force $F_{fr} = -V$ which describes in first approximation the relaxation of the cytoskeleton in moving cells.

(c) Cell–cell and cell–substrate adhesion responsible for sticking the cells together and on the surface are taken into account as a force slowing down the upward motion of cells: $(F_{ad})_z = -2V_z$; $(F_{ad})_x = (F_{ad})_y = 0$. Ideally, F_{ad} comes into action if somewhere inside of the mound the density of cells is slightly less than 1 and should be directed from the mounds-free surface up the cell density gradient. However, a force directed up to the cell density acts as a negative pressure and destabilises the computations. The method which we used to take F_{ad} into account behaves qualitatively correct. At least in the case of stable rotating and monotonic elongating mounds it avoids the formation of low cell density regions inside the mound and it is numerically stable.

(d) Pressure ($\mathrm{grad}p = 0.01\mathrm{grad}\rho$) in the aggregate develops when the cell density increases over a threshold value ($\rho > 1$) in this or in one of the six neighbouring grids (in the x-, y-, z-directions), while $\mathrm{grad}p = 0$ otherwise. This takes flows from high cell density regions as well as flows into surrounding regions of low cell density into account.

VISCOUS FLOW MODEL

Cell–Cell friction is taken into account by the use of two viscosity coefficients: $\eta = \rho$ and $\xi = 0.5\rho$. We assume that the force responsible for slowing down cell movement (the friction force F_{fr} in the first model) derives from the cell–substrate interaction. That is, $F_{fr} = -V$ for the cells located on the bottom plane and $F_{fr} = 0$ everywhere else. Cells moving on the bottom plane stop due to the friction with the substrate, while all other cells stop due to cell–cell friction (viscosity). This assumption results in more continuous cell movement in the mound in agreement with experimental observations (Fig. 6). However, cells in the lower part of the mound stop faster than cells in the upper part of the mound, which is not observed in experiments. To circumvent this problem we made one additional assumption, i.e. the chemotactic force is taken to be twice as strong for cells in contact with the substrate as for all other cells. This assumption results in roughly equal cell velocities everywhere in the mound.

The description of the force responsible for cell–cell and cell–substrate adhesion has also been improved. We take this force into account as a force directed towards the substrate ($(F_{ad})_z = 0.3$; $(F_{ad})_x = (F_{ad})_y = 0$) which occurs inside the mound in grid points where $\rho > 1$ when in grid point underneath $\rho < 1$. This force keeps the mound compact and dense also when the mound exhibits more complicated types of behaviour such as transformations of shape and meandering.

Inclusion of viscosity terms result in a smoother velocity profile in the mound but also decreases the

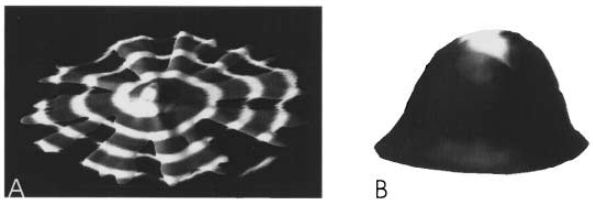

FIG. A1. Structures obtained in alternative models. (a) Aggregation pattern using the viscous flow model. Due to viscous cell–cell interactions the streams obtained in the viscous model and shown in (A) are much wider than obtained with the non-viscous model [Fig. 1(B)]. (B) Mound in the non-viscous flow model. The mound obtained with the non-viscous model is very flexible, and its surface is continuously deformed by the propagating cAMP waves. The version of non-viscous model used here differs from that used for Figs 1 and 2. The adhesive force is taken into account in the same way as in the viscous model (see Appendix C).

average velocity of the cells and therefore it also results in mound shape changes. We have chosen the values of the viscosity coefficients so that they are enough big to make the surface of the mound smooth (Figs 3 and 4) and increased chemotactic forces ($K_{ch} = 0.6$ in the bottom plane and $K_{ch} = 0.3$ in the rest of the space in the viscous model) to return to the hemispherical shape of the mound as shown in Fig. 3(A).

APPENDIX C
Variations of the Model

VISCOUS VS. NON-VISCOUS CELL FLOW

The results presented in Figs 1 and 2 can also be obtained using a viscous flow model, however, the morphology obtained is not as good. Using the viscous flow model to simulate aggregation results in the formation of too wide streams [Fig. A1(A)]. Using the non-viscous flow model to simulate non-stationary (moving or changing shape) mounds has problems as well. The shape of the mound is very flexible in this case and it is deformed by each cAMP wave propagating inside the mound [Fig. A1(B)]. We therefore conclude that the formation of aggregation streams is better described by using a non-viscous flow model, while mound behaviour is better approximated by a viscous flow model. This corresponds well to what is known about the strength of the cell–cell interactions in these stages (Loomis, 1982).

VELOCITY AND DENSITY PROFILES

Simulations with the viscous and non-viscous flow models show considerable differences in mound shape

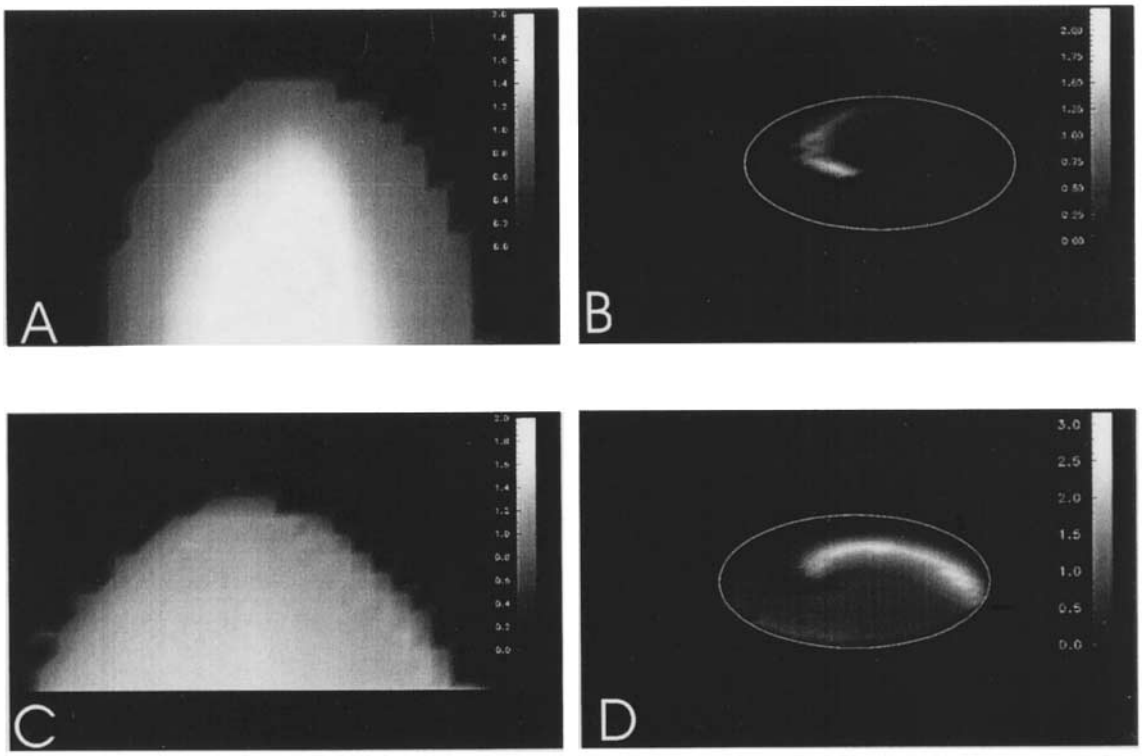

FIG. A2. Velocity and density profiles. (A,C) Density profiles of vertical cross-sections of the mounds shown in Fig. 1(D) and Fig. 3(A). The density of cells decreases from the centre of the mould to its boundary. The maximal density of cells is 2.1 in (A) and 1.6 in (B). (B,D) Velocity profiles for the bottom planes of the mounds in Fig. 1(D) and Fig. 3(A). The view point is the same as in Fig. 1(D). The velocity profiles are also spiral-shaped patterns and show that the cells in (D) move much longer than the cells in (B).

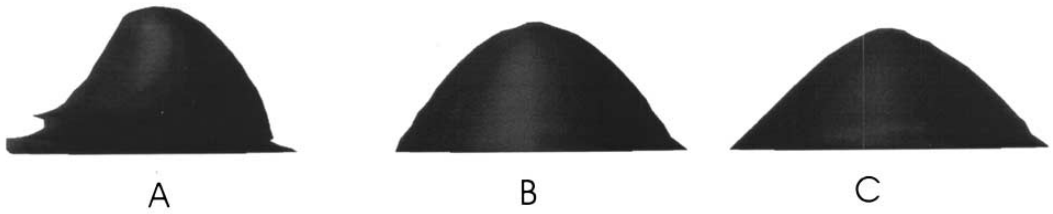

FIG. A3. Mounds in the viscous flow model with different chemotactic forcing. $K_{ch} = 0.6$ in (A); $K_{ch} = 0.3$ in (B); $K_{ch} = 0.15$ *in* (*C*). The mound in (B) is the same as in Fig. 3(A). The shape of the mound becomes flatter when K_{ch} decreases, and more elongated when it increases. The mound in (A) exhibits a meandering motion as shown for the mound in Fig. 3(B and C).

as well as in the velocity and density profiles inside the mound. Fig A2(A and C) show density distribution in a vertical cross-section of a non-viscous [Fig. 1(D)] and a viscous [Fig. 3(A)] mound. The shape of the non-viscous mound is much more pointed in comparison with the flat shape of the viscous mound. Cell density decreases smoothly from the centre of the mound to its periphery in both cases. The maximal cell density is higher in the non-viscous (2.1) than in the viscous model (1.6). By increasing the pressure we obtain a smoother density profile in the non-viscous mound due to a decrease of the maximal cell density inside the mound. It also results in changes of mound shape: it becomes more elongated. Fig. A2(B and D) show velocity profiles in the bottom sections of the mounds shown in Fig. A2(A and C). Cell movement results from the chemotactic force developing at the front of the cAMP wave. Therefore, the velocity profiles are also spiral-shaped, however, there is a significant difference in the relaxation time of the movement in these two cases. In non-viscous mound cells move only during a short time, while in the viscous mound the velocity of the cells drops much slower after a wave has passed, therefore, the cells move almost all the time. This behaviour is very similar to that seen under experimental conditions where cell movement has been shown to be almost continuous with only slight periodic modulations (Rietdorf *et al*., 1996).

VARIATION OF MODEL PARAMETERS

Here we briefly describe the main changes caused by variation of the model parameters. By variation of the parameters in equations (1)–(2) we can change excitability of the medium (Figs 2–4) and the shape of the cAMP waves. The change in wave shape can change the velocity of the chemotactic motion, since this velocity is roughly proportional to the duration of the rising phase of the cAMP wave. Increase in the coefficient of random cell motion, D_ρ results in an increase of the time of stream formation as well as in wider streams. It has almost no influence on the shape of the mound. The shape of the mound depends strongest on the parameters in eqn (3). A decrease in the chemotactic forcing, K_{ch}, or in viscosity coefficients, η and ξ, or in pressure, results in a flatter mound, while an increse in these parameters makes the mound elongated. The effects of changes in the chemotactic forcing on the shape of the mound are illustrated in Fig. A3. An increase in the friction term results in similar changes as a decrease in chemotactic forcing.